ACS APPLIED MATERIALS & INTERFACES

Letter

www.acsami.org

Gate-Tunable Photoresponse of Defective Graphene: from Ultraviolet to Visible

Kaliannan Thiyagarajan,[†] Balasubramaniam Saravanakumar,[†] and Sang-Jae Kim*[,†,‡]

[†]Nanomaterials and System Lab, Department of Mechatronics Engineering, Jeju National University, Jeju 690-756, Republic of Korea

[‡]School of Material Science and Engineering, Georgia Institute of Technology, Atlanta, Georgia 30332-0245, United States

Supporting Information

ABSTRACT: We report the gate-tunable photoresponse of a defective graphene over the ultraviolet (UV) and the visible light illumination, where the defect was generated by plasma irradiation. Plasma induced Dirac point shift indicates the p-doping effect. Interestingly the defective-graphene field effect transistor (defective-GFET) showed a negative shift upon UV illumination, whereas the device showed a positive shift under visible light illumination, along with the change in the photocurrent. The defective-GFET device showed a high photoresponsivity of 37 mA W^{-1} under visible light, that is ~3 times higher than that of the pristine graphene device. Photoinduced molecular desorption causes the UV light responsivity to 18 mA W^{-1}. This study shows that the tunable photodetector with high responsivity is feasible by introducing an artificial defect on graphene surface.

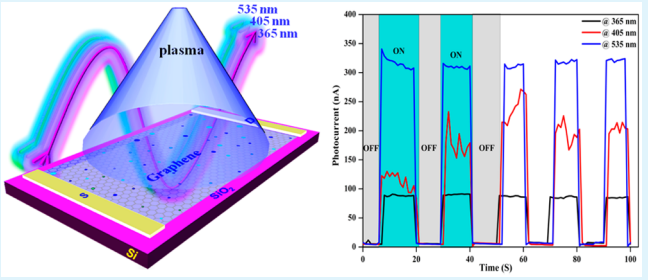

KEYWORDS: *graphene, field effect transistors, plasma irradiation, defects, photocurrent*

These days, photodetectors are made of different photoactive semiconductors with appropriate bandgaps,[1] to detect the wide spectral (ultraviolet to far-infrared) range, which is central to the imaging, sensing, and spectroscopic applications.[2] In contrast, the tunable bandgap in the fascinating two-dimensional graphene promises ultrabroadband photodetection[1,3,4] (ultraviolet to far-infrared) because of the electron hole pair generation upon a light irradiation over a broad spectrum.[1,5] Even though the photoresponsivity of the graphene photodetector was low, it is attributed to the poor absorption efficiency (2.3%) and short recombination lifetimes (~1.5 ps) of the photogenerated carriers.[3,6,7] To enhance the photoresponsivity of graphene, researchers have developed various modification schemes to extract photocurrent (PC), by chemical doping, thermo-electric effect,[8] metallic plasmonics,[9] graphene plasmons,[10] microcavities,[11] graphene quantum dots,[3,12] hybrid phototransistor,[13] and double-layer heterostructure photodetectors.[1] Apart from these techniques, inducing an artificial defect on the graphene lattice is another way of enhancing the PC.[7,14] Plasma[7] and ion irradiation (Ga^+ and Ar^+)[15] on graphene induces different types of surface defects such as vacancies, graphene islands, doping, and forming impurity by disrupting honeycomb lattice. These defects are acting as a scattering sites, which absorb the incident light better than the pristine, at the same time reduces the carrier recombination and facilitate continuous channel for charge carriers which significantly enhances the PC.[7,14]

In this letter, we demonstrate the gate-tunable photoresponse behavior of the defected graphene, over the ultraviolet to visible region. Where the plasma irradiation induces the defects. Depending on the illumination wavelength, the Dirac point of the device shifts to either side along with the change in the drain current, which engenders a novel way to tailor the photoresponse of the graphene.

Graphene was exfoliated from highly oriented pyrolytic graphite (HOPG) and the graphene field-effect transistor (GFET) device was fabricated by evaporating a 100 nm Au electrode on the photolithographically patterned graphene channel. Prior to plasma exposure, Raman spectrum (see Figure 1b (blue color)) and electrical measurements were carried out to ensure the properties of the pristine-GFET, and then the device was exposed to a custom-made atmospheric plasma reactor under Ar atmosphere with a flow rate of 60 sccm at a pressure of ~1 Torr for 1 min. For more details of the device fabrication, defect generation, and morphological analysis, see the Supporting Information (Experimental Section, Figures S1 and S2). The modification of the properties of the plasma-treated graphene (defected-graphene) was investigated.

Figure 1a is the schematic of the fabricated graphene FET device, where the pointlike structure in the graphene lattice represents the defects generated by plasma irradiation and the arrows represent the three different wavelengths used for the photocurrent measurement. The normalized Raman spectrum of the pristine (blue color) and defective (red color) GFET is shown in Figure 1b. The absence of the defect-related D peak and the appearance of G and 2D (graphitic) peaks, with an

Received: November 17, 2014
Accepted: January 14, 2015
Published: January 14, 2015

DOI: 10.1021/am507985m
ACS Appl. Mater. Interfaces 2015, 7, 2171−2177

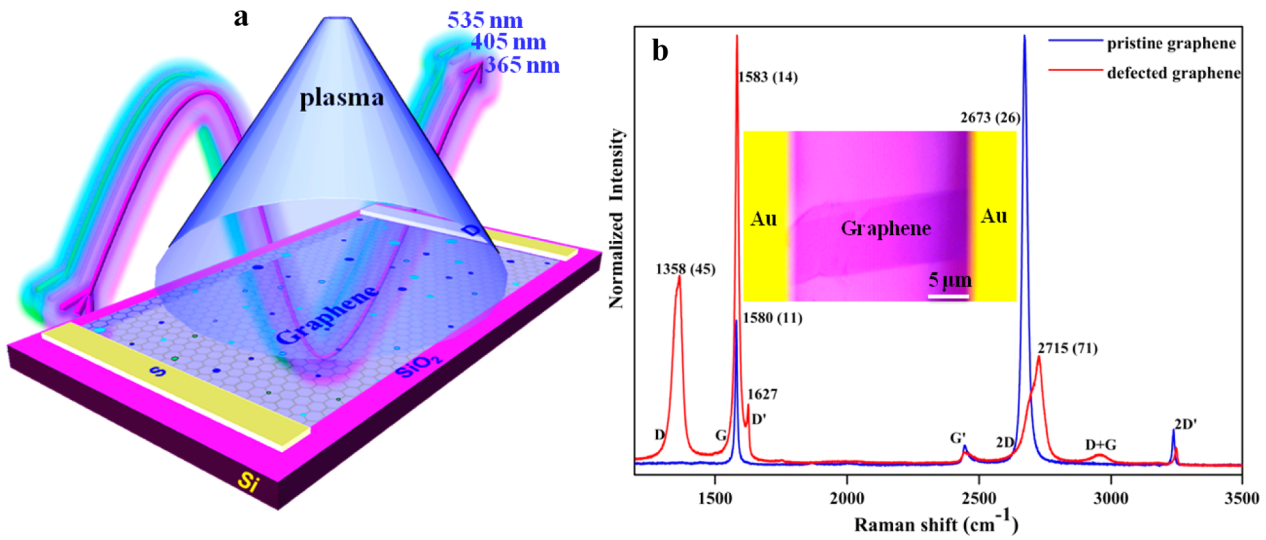

Figure 1. (a) Schematic representation of defect generation, and photoresponse of the fabricated graphene device (b) Normalized micro-Raman spectrum of the pristine and the defective graphene device, where the numbers denote the peaks positions and the numbers in the brackets are the full width half-maximum of the corresponding peaks. The inset is an optical microscopy image of a typical device.

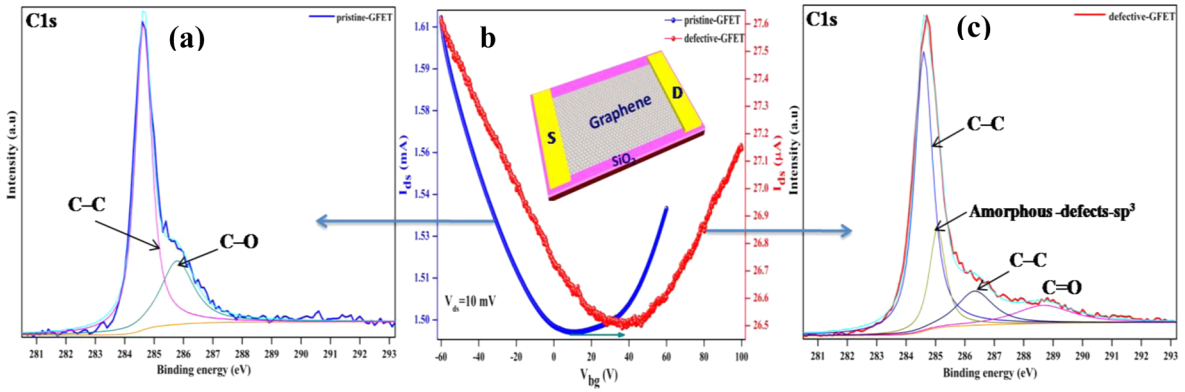

Figure 2. (a) C 1s high-resolution XPS spectra of the pristine −GFET device. (b) Transfer characteristics of the pristine and defective-GFET device at the drain source voltage of 10 mV. (c) C 1s high-resolution XPS spectra of the defective−GFET device, (Note that the spectra were deconvoluted using the Shirley method of background removal).

intensity ratio of 2.94, indicates that the device was successfully fabricated on a SiO_2/Si substrate without causing any material damage.[16] The inset in Figure 1b is the optical microscopy image of the fabricated GFET device. The appearance of defect-associated (D, D′, and D+G) peaks along with G and 2D peaks, in plasma-treated graphene, suggests that the A1g symmetry phonons near the K-zone became active[7] when the device was exposed into plasma. The existence of these defect-related peaks, with increments in the full-width at half-maximum (fwhm, numbers in the brackets) of the G and 2D peaks, along with the peak shift toward higher wave numbers, confirms the formation of structural defects,[7] which also suggested that the defects induce p-doping in the graphene device.[17]

To examine the electrical transformation of the defective GFET, we measured the transfer characteristics of the pristine and the defective GFET in room atmosphere with respect to back-gate voltage (V_{bg}) at a drain−source voltage (V_{ds}) of 10 mV; the result is depicted in Figure 2b. The pristine-GFET device (see the inset for the schematics) shows an ambipolar behavior with the Dirac point (V_{Dirac} charge neutrality point) at 8 V in the back-gate, which implies p-doping characteristics and which is due to the adsorbance of water and oxygen molecules on the graphene surface.[16] The Dirac point of the defective-GFET device is up-shifted to 39 V, which clearly suggests that the plasma treatment leads to increase the p-doping effect and introduces an asymmetry between electron and hole transport that is due to the accumulation of holes in graphene surface.[12] The plasma treatment introduces nanoscale defects in graphene surface, where the honeycomb lattice was broken by the synergistic effect of the plasma species,[18] and the defect sites reacted with the oxygen molecules (from atmosphere), making the device p-doped, which up-shifts the Dirac point to 39 V. The functional groups involved in the p-doping effect were obtained via X-ray photoelectron spectroscopy (XPS). Panels a and c in Figure 2 illustrate the C 1s core level spectra of pristine and defective GFET, respectively.

The spectra of pristine graphene fitted with two peaks, where the 284.6 eV peak belongs to the sp^2 hybridized carbon atom (C−C bond) and the other peak at 285.8 eV was assigned to the noncovalent C−O bond, may arise during device fabrication.[7] In contrast, the C 1s spectrum of defective graphene is fitted with four major components, where the higher-intensity peak at 284.6 eV, which is similar to that of the pristine; however, the spectrum differs when a peak emerges at

DOI: 10.1021/am507985m
ACS Appl. Mater. Interfaces 2015, 7, 2171−2177

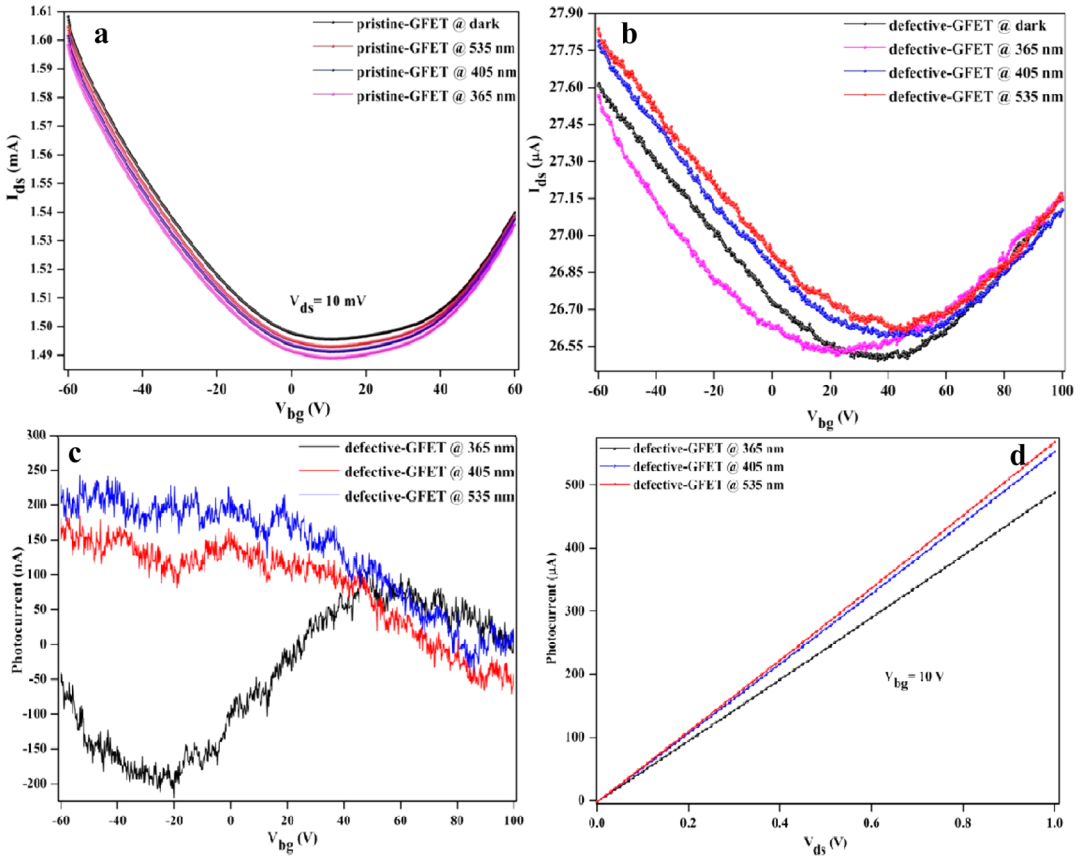

Figure 3. Transfer curves of the (a) pristine and (b) defective GFET device under different illumination wavelength. (c) Photocurrent as a function of back gate voltage based on the transfer curves obtained in b. (d) Photocurrent of the defective-GFET device with respect to the source-drain voltage, under the different illumination wavelength at constant V_{bg} = 10 V.

285.0 eV, which is attributed to the formation of sp^3-hybridized carbon atoms due to the removal of carbon atoms from the honeycomb lattice (amorphous defect generation).[19] The peak corresponds to C−O (286.3 eV), which has the possibility of forming epoxy and a hydroxyl group. For epoxy formation, which is one O atom bridging over two neighboring carbon atoms, the O 2p orbital strongly hybridizes with extended π π^* bands in graphene, which changes the carbon planar (sp^2) hybridization to distorted sp^3 hybridization.[20] In the case of hydroxyl formation, the O atom is on top of a carbon with C−O bond nearly perpendicular to the graphene plane, which causes the change in carbon hybridization from sp^2 to sp^3 by forming a strong covalent bond between C and O.[20] The peak at 288.5 eV ascribed to the formation of carbonyl bonds (C═O),[7] this may be a ketone. From the XPS spectra, it is clear that the p-doping behavior emerges in defective GFET, ascribed to the formation of hydroxyl, epoxy, and carbonyl functional groups which up-shifted the V_{Dirac} from 8 to 39 V. The plasma-induced defects sites are acting as light absorbing media in the photocurrent measurement.

Figure 3b shows the effect of light illumination on defective-GFET with different wavelength, where the Dirac point of the transfer curve in the dark is around 39 V, indicating the heavy p-doped nature of the device. When the device is illuminated by the visible light of 405 and 535 nm, the Dirac points shifted more toward the positive direction, along with the drain current increment (I_{ds}) in the p-channel, indicating further p-doping behavior.[12,17] On the other hand, when the Dirac point shifted toward the negative side and the I_{ds} in the p-channel decreased, the device is illuminated by UV light (365 nm), indicating n-doping behavior that is due to the photoinduced molecular desorption, which decreases the hole density in the defective-graphene channel.[21,22] There is no shift in the Dirac point of the pristine-GFET when illuminated with different wavelengths of light (see Figure 3a). The photocurrent dependence on gate voltage with respect to wavelength can be obtained by subtracting the dark current from the light current (I_{light} − I_{dark}) and the result is plotted in Figure 3c. It is clear that the gate-dependent photoresponse of the defective-GFET, can be tuned by illumination wavelength. The typical photoresponse of the defective-GFET device as a function of source−drain voltage (V_{ds}) under different illumination wavelengths (Figure 3d) with constant back gate voltage of 10 V is attributed to the effective separation of electron-hole pairs[1,12] in the defected graphene. For reference, we also measured the pristine-GFET device under the same conditions. No obvious response was observed, which was expected because of the poor absorbance and short recombination lifetime of the photogenerated carriers in defect-free graphene.[3,6,7]

For more insight into the Dirac point shifting and photoresponse behavior of the defective-GFET, we measured the gate dependence of photocurrent at different wavelength and power; see Figure 4a−c. The defective-GFET shows the strong photogating effect and gate modulation over the UV and visible region. The power-dependent photocurrent curves were extracted from Figure 3a−c and are plotted in Figure 4d−f. Here the photocurrent, lack in the polarity reversal, attributed to the accumulation of a large amount of holes (absorption of

DOI: 10.1021/am507985m
ACS Appl. Mater. Interfaces 2015, 7, 2171−2177

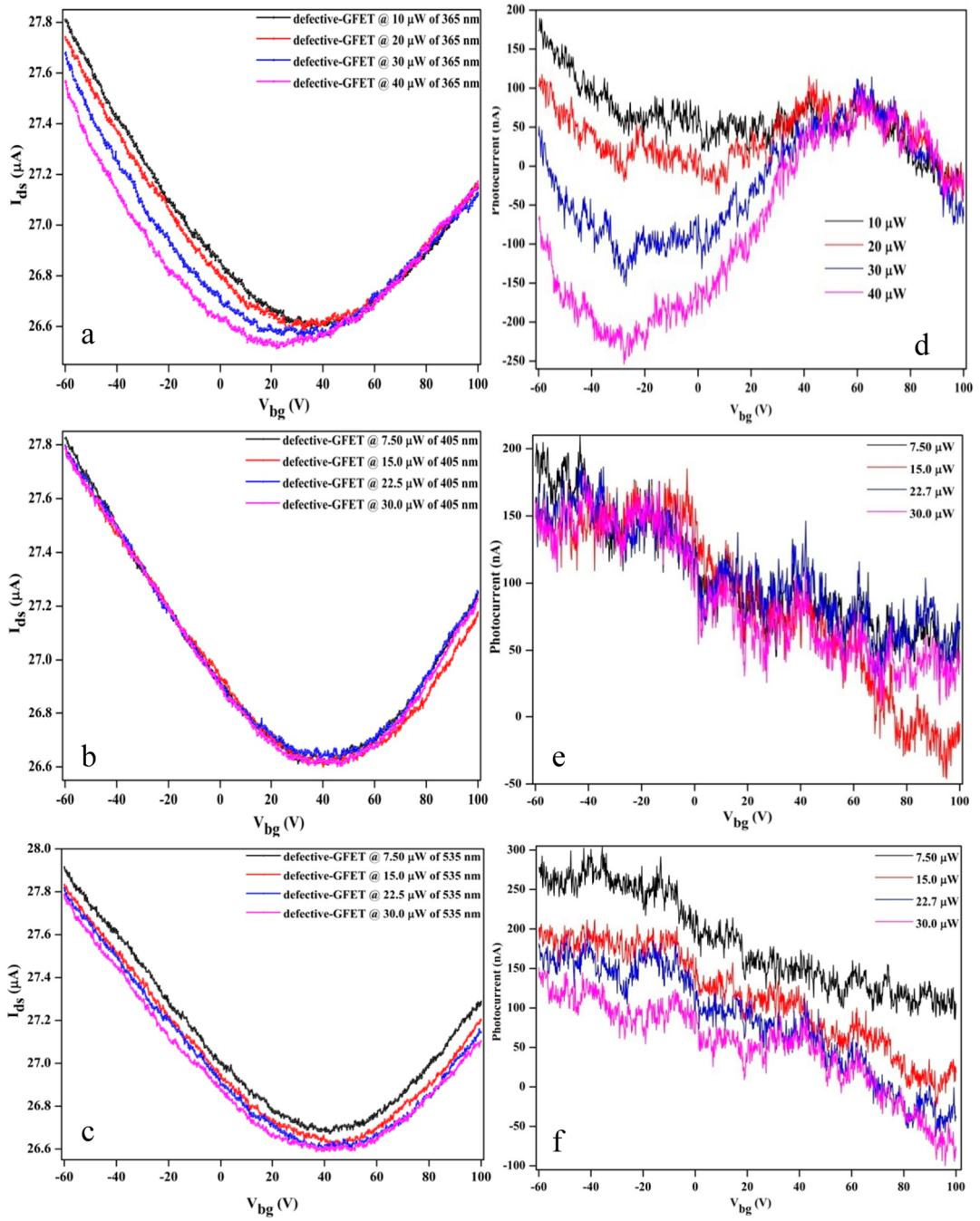

Figure 4. (a–c) Transfer curves of the defective-GFET device under different powers of 365, 405, and 535 nm light illumination, respectively. (d–f) Gate dependent photocurrent of the defective-GFET device under different powers of 365, 405, and 535 nm light illumination, respectively.

oxygen molecules)[12,21] in defected graphene causing the symmetry.

The photoinduced Dirac point shift (V_{Dirac}) in the defective-GFET with different powers of UV (365 nm) and visible (405 and 535 nm) light are shown in Figure 5a, a green dotted line indicates the Dirac point position in dark. When the device illuminated with visible (405 and 535 nm) light, the transferring of photogenerated holes to graphene induces further p-doping effect, which leads to an upshift in the V_{Dirac}, to 45 V for the power of 30 μW, the shift in the visible wavelengths (405 and 535 nm) are almost identical. Interestingly, the device showed down-shifts (toward negative) under UV (365 nm) light and Dirac point shifted to 22 V of V_{bg} for the power of 40 μW, which suggest that when the UV light is turned on, the photoinduced desorption process starts and the rate of the process increases when the incident power increases, resulted in n-doping (hole removal) effect.[21,22] The change in the charge carrier density (Δn) of the defective-GFET as a function of power is shown Figure 5b, where the charge carrier density is obtained based on the relation $\Delta n = ((\varepsilon\varepsilon_0)/(t_{ox}e))\,|V_{Di} - V_{DP}|$ where ε_o is the permittivity of free space, ε is the dielectric constant of SiO_2, t_{ox} is the thickness of the dielectric layer, e is electron charge, V_{DP} Dirac point of the defective GFET, V_{Di} Dirac point of the defective GFET[17,21] under light illumination. The value of Δn increases with increasing illumination power for all studied wavelengths, which is directly related to the

DOI: 10.1021/am507985m
ACS Appl. Mater. Interfaces 2015, 7, 2171–2177

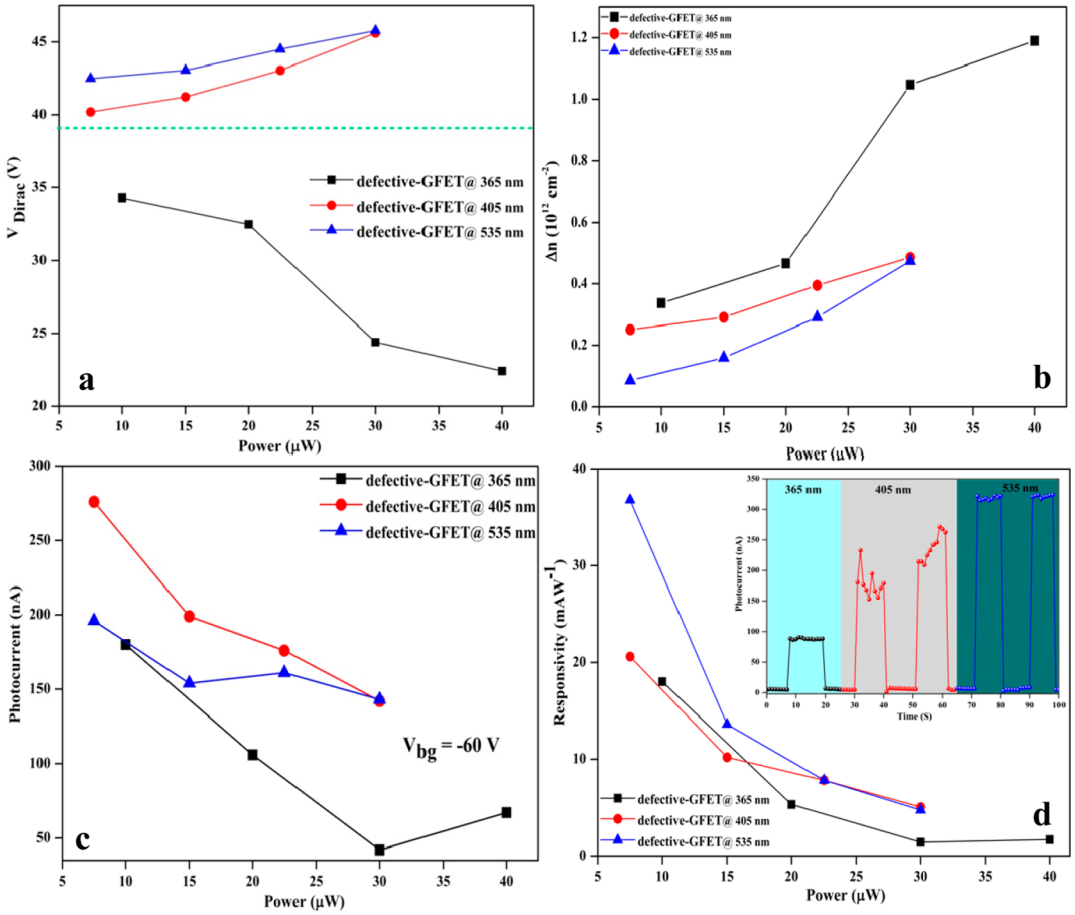

Figure 5. (a) Power-dependent Dirac point shift (V_{Dirac}) in the defective-GFET device (green dotted line indicates the Dirac point at dark). (b) Change in the charge carrier density of the defective-GFET as a function illumination power and wavelength. (c) Power-dependent photocurrent of the defective-GFET device at V_{bg} of −60 V. (d) Measured photoresponsivity versus powers under different illumination wavelength, the inset is the time-dependent photocurrent spectra of the defective-GFET device under UV (365 nm) and visible (405 and 535 nm) light irradiation for a bias of 1 V, at V_{bg} = 0 V.

Table 1. Comparison of the Photoresponsivity of Graphene Transistors in the UV and Visible Region

detector type	active layer	wavelength	responsivity	ref
	SLG	632.8 nm	1 mA/W	24
	SLG	532 nm	~10 mA/W	25
	BLG	480−750 nm	~1.5 mA/W	8
	SLG	690 nm	0.25 mA/W	26
visible	SLG/$FeCl_3$−FLG	532 nm	~0.1 V/W	27
	SLG/metal nanostructures	457−785 nm	~10 mA/W	9
	SLG/chlorophyll	683 nm	~1.1 × 10^6A/W	28
	SLG/argon plasma	535 nm	~37 mA/W	present work
	SLG/argon plasma	405 nm	~21 mA/W	present work
	SLG/MoS_2	635 nm	5 × 10^8 A/W	29
UV	SLG/ZnO QDs	325 nm	1 × 10^4 A/W	30
	SLG/argon plasma	365 nm	~18 mA/W	present work

[a]SLG, single layer graphene; BLG, bilayer graphene; FLG, few layer graphene.

tenability of the Fermi level of the graphene layers. Figure 5c shows the photocurrent of the defective-GFET device as a function of incident power with various illumination wavelengths, at V_{bg} of −60 V, where the V_{ds} is 10 mV. The photocurrent of the device decreases with respect to the power, for all illumination wavelengths, which is due to the high defect density,[14,21] trapping of holes in the defected sites,[7] as well as the fast recombination of photogenerated charge carriers.[3] The high illumination power, required high external bias voltage to separate the excitons, before they recombine,[23] which may increase the photoresponse of the device, because the device shows a linear reponse in the $I_{ds} - V_{ds}$ curve, see Figure 3d.

The significant parameter to determine the capability of a photodetector or photoconductor is responsivity (R), which depends on the electrical output to the optical input. R is defined as[2,7,12]

DOI: 10.1021/am507985m
ACS Appl. Mater. Interfaces 2015, 7, 2171−2177

$$R(AW^{-1}) = \frac{(I_{light} - I_{dark})}{P_{opt}} \quad (1)$$

where I_{light}, I_{dark}, P_{opt}, are current under illumination, current in dark, and incident light power, respectively. The responsivity of the defective-GFET device is estimated using eq 1. The device shows high responsivity under low excitation power, and we achieved values of 37, 21, and 18 mA W^{-1} for 535, 405, and 365 nm wavelengths, respectively (see Figure 5d) at 10 mV source-drain bias voltage (V_{ds}). This high photoresponsivity of the device is due to the effective separation of photogenerated electron−hole pair in the defected graphene surface.[3,7] Now it's clear that the defective-GFET device has the capability of converting the incident photons into electrical signal for broad spectral wavelength. The photoresponsivity of our device is very much comparable with the previous reports, see Table 1, where the FET-based photoresponsivity of the mechanically exfoliated graphene layers was compared over the UV and visible region.

The inset in Figure 5d shows the time-dependent photocurrent measurement of the defective-GFET device under UV (365 nm) and visible (405 and 535 nm) light modulation with 1 V bias voltage, at room temperature, where the V_{bg} is 0 V. Here the turn-on and turn-off time of the light source was 10 s. The device showed excellent stability and reproducibility over UV and visible region see Figure S3 (Supporting Information). The ratio of I_{light} to I_{dark} increased as the illumination wavelength, increased, having values of 86, 240, and 320, for wavelengths of 365, 405, and 535 nm, respectively. The device showed a fast switching; when the light source was turned on, the photocurrent reaches its maximum level within 0.9 s and the decay time of the device is 1 s. These are very much comparable to the previous reports.[14,21] The high photoresponsivity and fast switching time in the defective-GFET devices suggest that it can be employed for photodetection applications.

In summary, we report an enhanced, stable, wavelength-dependent, and gate-tunable photoresponse in graphene by inducing defects by plasma irradiation. Raman, X-ray photoelectron spectroscopy, and electrical transport measurement showed that plasma irradiation imposes p-doping. The effective separation of photoinduced charge carriers in the defect site enhances the photoresponse of the defective-GFET device, except the higher power regions. The device shows high responsivity under low excitation power, and a maximum photoresponsivity of 37 mA W^{-1} for 535 nm illumination, which is ∼3 times higher than that of the pristine graphene. Photoinduced molecular desorption under 365 nm UV light illumination causes the responsivity to 18 mA W^{-1}. The photoresponse of the defected graphene could be further enhanced by controlling the defect density. This study shows that the tunable photodetector with high responsivity is feasible by introducing an artificial defect on graphene surface.

■ ASSOCIATED CONTENT

Supporting Information

Detailed explanation of the device fabrication and the plasma irradiation condition (defect generation); atomic force microscopy (AFM) analysis (surface morphology) of pristine and defected graphene; time-dependent photocurrent measurement of the defective-GFET device with multiple on/off cycles. This material is available free of charge via the Internet at http://pubs.acs.org/.

■ AUTHOR INFORMATION

Corresponding Author

*E-mail: kimsangj@jejunu.ac.kr; sang.kim@mse.gatech.edu. Tel: +82-64-754-3715. Fax: +82-64-756-3886.

Notes

The authors declare no competing financial interest.

■ ACKNOWLEDGMENTS

This research was supported by the Basic Science Research Program through the National Research Foundation of Korea (NRF) funded by the Ministry of Science, ICT, and Future Planning (2013R1A2A2A01068926).

■ REFERENCES

(1) Liu, C. H.; Chang, Y. C.; Norris, T. B.; Zhong, Z. Graphene Photodetectors with Ultra-Broadband and High Responsivity at Room Temperature. *Nat. Nanotechnol.* **2014**, *9*, 273−278.

(2) Li, J.; Niu, L.; Zheng, Z.; Yan, F. Photosensitive Graphene Transistors. *Adv. Mater.* **2014**, *26*, 5239−5273.

(3) Zhang, Y.; Liu, T.; Meng, B.; Li, X.; Liang, G.; Hu, X.; Wang, Q. J. Broadband High Photoresponse from Pure Monolayer Graphene Photodetector. *Nat. Commun.* **2013**, *4*, 1811.

(4) Mak, K. F.; Ju, L.; Wang, F.; Heinz, T. F. Optical Spectroscopy of Graphene: from the Far Infrared to the Ultraviolet. *Solid State Commun.* **2012**, *152*, 1341−1349.

(5) Sargent, E. H. A Sensitive Pair. *Nat. Nanotechnol.* **2012**, *7*, 349−350.

(6) Breusing, M.; Ropers, C.; Elsaesser, T. Ultrafast Carrier Dynamics in Graphite. *Phys. Rev. Lett.* **2009**, *102*, 086809.

(7) Thiyagarajan, K.; Ananth, A.; Saravanakumar, B.; Mok, Y. S.; Kim, S. J. Plasma-Induced Photoresponse in Fewlayer Graphene. *Carbon* **2014**, *73*, 25−33.

(8) Lemme, M. C.; Koppens, F. H. L.; Abram, L. F.; Rudner, M. S.; Park, H.; Levitov, L. S.; Marcus, C. M. Gate-Activated Photoresponse in a Graphene p-n Junction. *Nano Lett.* **2011**, *11*, 4134−4137.

(9) Echtermeyer, T. J.; Britnell, L.; Jasnos, P. K.; Lombardo, A.; Gorbachev, R. V.; Grigorenko, A. N.; Geim, A. K.; Ferrari, A. C.; Novoselov, K. S. Strong Plasmonic Enhancement of Photovoltage in Graphene. *Nat. Commun.* **2011**, *2*, 458.

(10) Koppens, F. H. L.; Chang, D. E.; Garcia, de; Abajo, F. J. Graphene Plasmonics: a Platform for Strong Light−Matter Interactions. *Nano Lett.* **2011**, *11*, 3370−3377.

(11) Engel, M.; Steiner, M.; Lombardo, A.; Ferrari, A. C.; Löhneysen, H. V.; Avouris, P.; Krupke, R. Light−Matter Interaction in a Microcavity-Controlled Graphene Transistor. *Nat. Commun.* **2012**, *3*, 906.

(12) Cheng, S. H.; Weng, T. M.; Lu, M. L.; Tan, W. C.; Chen, J. Y.; Chen, Y. F. All Carbon-Based Photodetectors: An Eminent Integration of Graphite Quantum Dots and Two Dimensional Graphene. *Sci. Rep.* **2013**, *3*, 2694.

(13) Konstantatos, G.; Badioli, M.; Gaudreau, L.; Osmond, J.; Bernechea, M.; Pelayo Garcia de Arquer, F.; Gatti, F.; Koppens, F. H. L. Hybrid Graphene−Quantum Dot Phototransistors with Ultrahigh Gain. *Nat. Nanotechnol.* **2012**, *7*, 363−368.

(14) Gowda, P.; Sakorikar, T.; Reddy, S. K.; Ferry, D. B.; Misra, A. Defect-Induced Enhancement and Quenching Control of Photocurrent in Few-Layer Graphene Photodetectors. *ACS Appl. Mater. Interfaces* **2014**, *6*, 7485−7490.

(15) Al-Harthi, S. H.; Karàa, A.; Hysen, T.; Elzain, M.; Al-Hinai, A. T.; Myint, M. T. Z. Evolution of Surface Morphology and Electronic Structure of Few layer Graphene After Low Energy Ar^+ Ion Irradiation. *Appl. Phys. Lett.* **2012**, *101*, 213107.

DOI: 10.1021/am507985m
ACS Appl. Mater. Interfaces 2015, 7, 2171−2177

(16) Thiyagarajan, K.; Saravanakumar, B.; Mohan, R.; Kim, S. J. Self-Induced Gate Dielectric for Graphene Field-Effect Transistor. *ACS Appl. Mater. Interfaces* **2013**, *5*, 6443−6446.
(17) Iqbal, M. Z.; Khan, M. F.; Iqbal, M. W.; Eom, J. Tuning the Electrical Properties of Exfoliated Graphene Layers using Deep Ultraviolet Irradiation. *J. Mater. Chem. C* **2014**, *2*, 5404−5410.
(18) Rousseau, B.; Szwarckopf, H. E.; Thomann, A. L.; Brault, S. P. C-Atom Displacements on HOPG Surface Under Plasma Low-Energy Argon-Ion Bombardment. *Appl. Phys. A: Mater. Sci. Process.* **2003**, *77*, 591−597.
(19) Su, Y.; Pei, S.; Du, J.; Liu, W. B.; Liu, C.; Cheng, H. M. Patterning Flexible Single-Walled Carbon Nanotube Thin Films by an Ozone Gas Exposure Method. *Carbon* **2013**, *53*, 4−10.
(20) Yan, J. A.; Chou, M. Y. Oxidation Functional Groups on Graphene: Structural and Electronic Properties. *Phys. Rev. B* **2010**, *82*, 125403.
(21) Kang, C. G.; Lee, S. K.; Choe, S.; Lee, Y. G.; Lee, C. L.; Lee, B. H. Intrinsic Photocurrent Characteristics of Graphene Photodetectors Passivated with Al_2O_3. *Opt. Express* **2013**, *21*, 23391−23400.
(22) Sun, P.; Zhu, M.; Wang, K.; Zhong, M.; Wei, J.; Wu, D.; Cheng, Y.; Zhu, H. Photoinduced Molecular Desorption from Graphene Films. *Appl. Phys. Lett.* **2012**, *101*, 053107.
(23) Gowda, P.; Mohapatra, D. R.; Misra, A. Enhanced Photoresponse in Monolayer Hydrogenated Graphene Photodetector. *ACS Appl. Mater. Interfaces* **2014**, *6*, 16763−16768.
(24) Xia, F.; Mueller, T.; Mojarad, G. R.; Freitag, M.; Lin, Y.; Tsang, J.; Perebeinos, V.; Avouris, P. Photocurrent Imaging and Efficient Photon Detection in a Graphene Transistor. *Nano Lett.* **2009**, *9*, 1039−1044.
(25) Park, J.; Ahn, Y. H.; Vargas, C. R. Imaging of Photocurrent Generation and Collection in Single-Layer Graphene. *Nano Lett.* **2009**, *9*, 1742−1746.
(26) Freitag, M.; Low, T.; Xia, F.; Avouris, P. Photoconductivity of Biased Graphene. *Nat. Photon.* **2013**, *7*, 53−59.
(27) Withers, F.; Bointon, T. H.; Craciun, M. F.; Russo, S. All-Graphene Photodetectors. *ACS Nano* **2013**, *7*, 5052−5057.
(28) Chen, S. Y.; Lu, Y. Y.; Shih, F. Y.; Ho, P. H.; Chen, Y. F.; Chen, C. W.; Chen, Y. T.; Wang, W. H. Biologically Inspired Graphene-Chlorophyll Phototransistors with High Gain. *Carbon* **2013**, *63*, 23−29.
(29) Roy, K.; Padmanabhan, M.; Goswami, S.; Sai, T. P.; Ramalingam, G.; Raghavan, S.; Ghosh, A. Graphene−MoS_2 Hybrid Structures for Multifunctional Photoresponsive Memory Devices. *Nat. Nanotechnol.* **2013**, *8*, 826−830.
(30) Guo, W.; Xu, S.; Wu, Z.; Wang, N.; Loy, M. M. T.; Du, S. Oxygen-Assisted Charge Transfer between ZnO Quantum Dots and Graphene. *Small* **2013**, *9*, 3031−3036.

DOI: 10.1021/am507985m
ACS Appl. Mater. Interfaces 2015, 7, 2171−2177